Journal of Membrane Science 353 (2010) 85–93

Contents lists available at ScienceDirect

Journal of Membrane Science

journal homepage: www.elsevier.com/locate/memsci

Modelling the simultaneous heat and mass transfer of direct contact membrane distillation in hollow fibre modules

V.A. Bui[a,1], L.T.T. Vu[b], M.H. Nguyen[c,d,*]

[a] Centre for Plant and Food Science, University of Western Sydney, NSW, Australia
[b] School of Engineering and Energy, Murdoch University, WA, Australia
[c] School of Natural Sciences, University of Western Sydney, NSW, Australia
[d] School of Environmental and Life Sciences, University of Newcastle, NSW, Australia

ARTICLE INFO

Article history:
Received 23 September 2009
Received in revised form 8 February 2010
Accepted 10 February 2010
Available online 18 February 2010

Keywords:
Direct contact membrane distillation
DCMD
Modelling
Hollow fibre
Shell side heat and mass transfer

ABSTRACT

This paper presents a new procedure for modelling the simultaneous heat and mass transfer in direct contact membrane distillation (DCMD) in a hollow fibre configuration. Iterative calculations in classic dimensionless analysis were applied to develop semi-empirical models, employing the analogy between heat and mass transfer. The procedure incorporated the significant effect of the membrane module's geometry: length and tortuosity of fibres in the bundle and fibres' size. Additionally, the new procedure showed the influence of the exponent β of Prandtl and Schmidt numbers on the validity of the models to simultaneously describe heat and mass transfer in the DCMD process. Current results agreed well with other analyses in the literature. The value close to 0.33 of β, as conventionally used, could be applied for heat transfer and minimal mass transfer. In other more intensive mass transfer cases, it was found that the values of β could go up to 0.55. The new models demonstrated a linear relationship between heat and mass fluxes and their respective driving forces, namely conductive heat flux against temperature gradient and mass flux against water vapour pressure difference across the membrane. Finally these semi-empirical models were applied to evaluate the performance of various hollow fibre modules of different length and types.

1. Introduction

Direct contact membrane distillation (DCMD) is a selective membrane separation process driven by a vapour pressure gradient across a *hydrophobic microporous membrane*. The driving force for mass transfer in DCMD is created by the temperature difference across the membrane between a hot solution, *the feed*, and the cold permeate which is usually pure water. The membrane must be hydrophobic to avoid penetration of any liquid into the membrane pores. These pores are hypothetically filled with stagnant air. As a water vapour pressure gradient is formed across the pores, water molecules start to evaporate from the gas–liquid interface on the feed side, diffuse through the immobilised air in the pores, condense on the permeate side, and eventually are swept away with the permeate stream [1]. Due to the presence of a temperature difference across the membrane, heat and mass transfer simultaneously occur. As a result, multiple polarisations exist in DCMD as demonstrated in Fig. 1. All symbols and abbreviations used in this figure and throughout the paper are shown in the nomenclature list.

DCMD has attracted interest from the research community due to its simplicity and ease of implementation, possibility of utilising waste heat, and a high potential of applicability in a wide range of areas [2]. This process has mostly been studied for application in desalination, waste water treatment and concentration of aqueous solutions [3] where removal of water from the feed is the main concern. DCMD also appears to be suitable for concentration of thermally sensitive liquid foods as it has demonstrated the ability to operate at low temperatures, and yet achieved high solid contents [4–7].

However, low temperature DCMD has not been commercially practised due to its energy inefficiency [8–10]. Therefore, modelling of heat and mass transfer in DCMD is required as a prerequisite step for simulation and optimisation aiming at reducing the energy consumption in the process. This paper focuses on a better modelling method for the transport processes in DCMD.

Previous attempts [11,12] to model the flux in DCMD used a value of 0.33 for the exponent β of Prandtl and Schmidt numbers in

* Corresponding author at: University of Western Sydney, School of Natural Sciences, Bourke Street, Hawkesbury Campus, UWS Locked Bag 1797, Penrith South, NSW 1797, Australia. Tel.: +61 245701343.
E-mail address: minh.nguyen@newcastle.edu.au (M.H. Nguyen).
[1] Current address: Faculty of Food Science and Technology, Nong Lam University, Viet Nam.

0376-7388/$ – see front matter © 2010 Elsevier B.V. All rights reserved.
doi:10.1016/j.memsci.2010.02.034

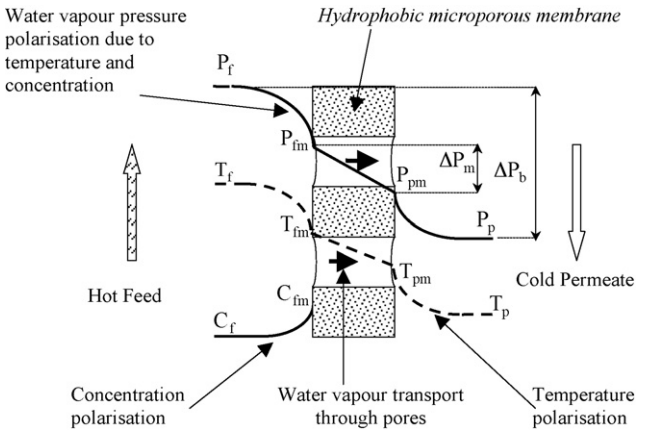

Fig. 1. Multiple polarisations in a DCMD process.

the calculations of Nusselt and Sherwood numbers and they had not been quite satisfactory. Different values of β that better describe the coupled heat and mass transfer in the process will be determined by a new method based on dimensional analysis. In the following sections, the configuration and model of a DCMD process will be presented, the problem will be formulated and solved for the new values of β. The model will be tested for its fitness in describing heat and mass transfer of a DCMD operation to concentrate a glucose solution by different hollow fibre modules (HFM). It will also be used to evaluate the different HFM types.

2. Heat and mass transfer in DCMD in hollow fibre configuration

For a hollow fibre configuration as in this study, heat and mass fluxes through the boundary layers and the total heat exchanged between the feed and the permeate are shown in Fig. 2. Temperature and concentration profiles in this figure are dependent on the flow characteristics of the two streams and the heat and mass exchanges between them. Once these profiles have been determined the transmembrane water vapour pressure (WVP), which is the mass transfer driving force of the DCMD process, can be estimated by the well-known Antoine equation for pure water (the permeate) and the relationship between water activity, a_w, of an aqueous solution and its WVP (the feed). These equations are well documented in the literature and can be found in Refs. [13–15] for example. Subsequently, Eq. (1) is commonly applied in the calculation of DCMD mass flux. Other applicable mechanisms include the Schofield model [16] and the Dusty-gas model [17] but they will not be needed here.

$$J = K_m(P_{fm} - P_{pm}) = \frac{1}{Y_{lm}} \frac{K_1 D_{w\text{-}air}}{r_i \ln(r_o/r_i)} \frac{M}{RT_m} \Delta P_m = K_M \Omega \, \Delta P_m \quad (1)$$

where

$$\Omega = \frac{D_{w\text{-}air}}{Y_{lm}} \frac{M}{RT_m}; \quad K_M = \frac{K_1}{r_i \ln(r_o/r_i)}; \quad K_m = K_M \Omega \quad (2)$$

In Eq. (1), J is the mass flux, based on the internal surface area of the fibres; $K_1 = \varepsilon/\tau$, a membrane quality parameter, with ε being the membrane porosity and τ being pore tortuosity; and K_M, a membrane's structural parameter. In this equation, the membrane vapour permeability K_m can be estimated by the molecular diffusion law, modified for the cylindrical geometry of hollow fibres. This mechanism of vapour transport is considered the simplest, requiring the least input parameters, and has been successfully applied in a number of studies in DCMD on flat sheet membrane.

After the mass flux, the concentration of the feed and the temperatures at both membrane surfaces need to be determined. For this step, only a heat transfer model is needed on the permeate side while both heat and mass transfer models are required on the shell (feed) side.

Hollow fibre module (HFM) is a configuration consisting of a bundle of hollow fibres housed in a shell. Although the fibres in the modules are not ideally straight, a flow of liquid inside the fibres, called the lumen side, can be considered as similar to that in cylindrical pipes. Thus, by allowing the cold water permeate to flow inside the fibres, readily available semi-empirical heat transfer models for a flow inside cylindrical pipes can be applied. This simplification however cannot be made for the feed flow in the shell side due to the random distribution of fibres in this flow channel. Thus, modelling of heat and mass transfer in the shell side of a hollow fibre module became the focus in this study.

As one of many membrane processes, "thin film theory" can be applied for the description of mass transfer in the feed boundary layer in DCMD. The validity of this theory has been well demonstrated in a number of numerical studies on DCMD and reverse osmosis, using the finite element approach [18–20]. There is a similarity between reverse osmosis and DCMD in that only water is being removed through the film layer next to the membrane surface. As a result, feed concentration at the membrane's surface in a hollow fibre configuration could be determined as in Eq. (3). This theory has been used extensively in mass transfer analysis of mem-

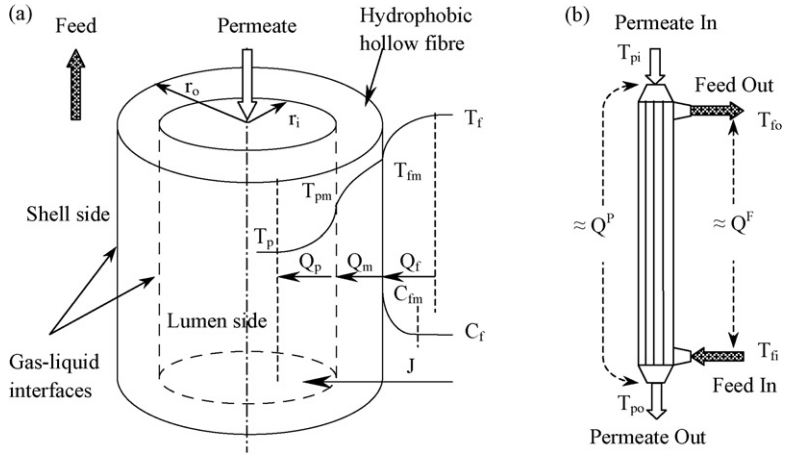

Fig. 2. DCMD heat and mass fluxes through boundary layers in hollow fibres (a) and total heat exchanged between feed and permeate (b).

Table 1
Analogous dimensionless numbers in heat and mass transfer models.

In heat transfer model	In mass transfer model
Nusselt: $\mathrm{Nu} = \frac{hd_h}{k}$	Sherwood: $\mathrm{Sh} = \frac{Kd_h}{D_{S\text{-}W}}$
Reynolds: $\mathrm{Re} = \frac{\omega d_h \rho}{\mu}$	Reynolds: $\mathrm{Re} = \frac{\omega d_h \rho}{\mu}$
Prandtl: $\mathrm{Pr} = \frac{C_p \mu}{k}$	Schmidt: $Sc = \frac{\mu}{\rho D_{S\text{-}W}}$
Model: $\mathrm{Nu} = \text{function}(Re^{\alpha}, \mathrm{Pr}^{\beta}, \text{geometry})$	Model: $\mathrm{Sh} = \text{function}(\mathrm{Re}^{\alpha}, \mathrm{Sc}^{\beta}, \text{geometry})$

brane distillation [21,22]; and osmotic distillation [23,24].

$$C_{fm} = C_f \exp\left(\frac{J r_i / r_o}{\rho_f K_f}\right) \tag{3}$$

In Eq. (3), the convective mass transfer coefficient K_f was estimated by applying the semi-empirical mass transfer model which was assumed to be analogous to the heat transfer model in the same domain. This assumption is generally accepted due to the similarity of the two transport processes occurring in the same geometry [25,26]. The analogy is detailed in Table 1 with the models which needed to be developed.

Based on the principle of convective heat transfer and the simultaneous occurrences of heat and mass transfer in DCMD, the heat balance of the system could be described as below in Eqs. (4)–(10):

- Total heat lost by the feed and gained by the permeate due to temperature changes from the inlets to the outlets of the corresponding streams:

$$Q^F = \dot{m}_f C_{pf}(T_{fi} - T_{fo}) \tag{4}$$

$$Q^P = \dot{m}_p C_{pp}(T_{po} - T_{pi}) \tag{5}$$

Neglecting the loss of heat through the HFM's insulation, the heat fluxes ascertained by Eqs. (4) and (5) should be the same, hence an average was accepted as indicative of the total heat exchanged between the feed and the permeate in the DCMD process:

$$Q_T = 0.5 \times (Q^F + Q^P) \tag{6}$$

- Heat fluxes through the boundary layers due to convection:

$$Q_f = A_o h_f (T_f - T_{fm}) \tag{7}$$

$$Q_p = A_i h_p (T_{pm} - T_p) \tag{8}$$

- Heat flux through the membrane Q_m. This heat flux included not only the conductive heat flux, but also the latent heat of water vapour transferred across the membrane:

$$Q_m = A_i h_m (T_{fm} - T_{pm}) + A_i J \Delta H_v \tag{9}$$

- Overall heat balance of the system:

$$Q_T = Q_p = Q_f = Q_m \tag{10}$$

The overall heat transfer coefficient was estimated as given in Eq. (11) with $\Delta T_m = T_{fm} - T_{pm}$:

$$U = \left(\frac{1}{h_p} + \frac{1}{h_m + (J\Delta H_v)/\Delta T_m} + \frac{1}{h_{f'}}\right)^{-1}; \quad \text{where } h_{f'} = h_f \frac{r_o}{r_i} \tag{11}$$

In the equations above, all heat and mass fluxes were based on the internal surface area of the fibres. Mean temperatures of the feed and permeate streams were approximated from the measured inlet and outlet temperatures as demonstrated in Eq. (12), while the conductive heat transfer coefficient of the porous membrane, h_m, was estimated by Eq. (13), for cylindrical geometry of the hollow fibres, as based on its constituents—air and polymer:

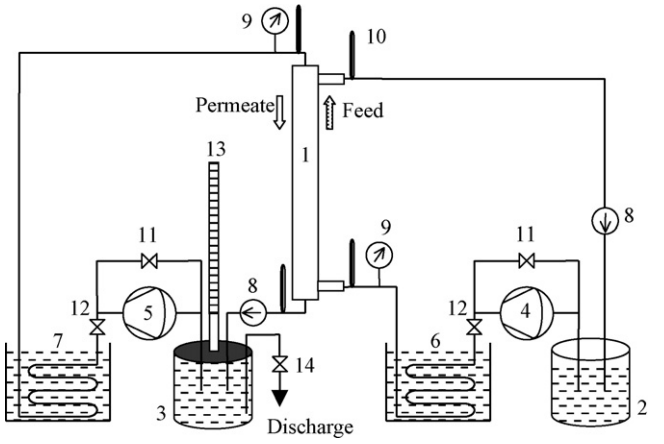

Fig. 3. Schematic diagram of the lab-scale DCMD unit using HFMs. (1, HFM; 2, feed bottle; 3, permeate bottle; 4 and 5, pumps; 6, hot water bath; 7, cool water bath; 8, flow meters; 9, pressure gauges; 10, thermometers; 11 and 12, flow regulating valves; 13, flux recording pipette; 14, permeate discharge valve).

$$T_f = \frac{T_{fi} + T_{fo}}{2} \quad \text{and} \quad T_p = \frac{T_{pi} + T_{po}}{2} \tag{12}$$

$$h_m = \frac{k_m}{r_i \ln(r_o/r_i)} = \frac{\varepsilon k_{air} + (1-\varepsilon) k_{pl}}{r_i \ln(r_o/r_i)} \tag{13}$$

3. Experimental setup

Experiments were carried out on a lab-scale DCMD unit shown in Fig. 3, concentrating glucose solutions of 30, 40, 50 and 60% (w/w) at temperatures of 25, 30, 35 and 40 °C at the feed inlet. Details of the hollow fibre modules PVDF (PV modules) and Halar (HL modules) used in the DCMD unit are specified in Table 2.

Feeds were glucose solutions, flowing in the shell side of the hollow fibre module at different velocities up to 0.8 m s^{-1}. Permeate was pure water, flowing in the lumen side at a maximal constant velocity of 1.2 m s^{-1} and at constant inlet temperature of 10 °C. Due to the pressure limits of the membranes, the feed velocity could not go above 0.8 m s^{-1}. During the experiments, the mass of water transferred from the feed into permeate over a period of 15 min was precisely measured by the water level rising in pipette 13. This amount of water was then discharged via valve 14 back into bottle 2 to maintain a constant feed concentration in subsequent experiments. The temperatures at the inlets of the feed and permeate streams were controlled to the aforementioned levels, while those at the outlets were measured by thermometer 10 and recorded. The heat and mass transfer data were calculated following the steps described in Section 4 below.

4. Procedure for modelling heat and mass transfer in DCMD

On the permeate side, heat transfer models for a laminar flow ($\mathrm{Re} < 2100$) within a cylindrical pipe, expressed as Eqs. (14[a]) and (14[b]), were applied [27–29]:

- Sieder–Tate model:

$$\mathrm{Nu}_p = 1.86\left(\mathrm{Re}_p \mathrm{Pr}_p \frac{d_{hp}}{L}\right)^{0.33} \times \left(\frac{\mu_p}{\mu_{pm}}\right)^{0.14} \quad \text{if}$$

$$\mathrm{Gz}_p = \mathrm{Re}_p \mathrm{Pr}_p \frac{d_{hp}}{L} \geq 100 \tag{14[a]}$$

Table 2
Specifications of the hollow fibre modules used in DCMD experiments.

Code	n	ϕ (%)	d_i (mm)	L (mm)	L_T (mm)	A_i (cm^2)	A_l (mm^2)	A_{sh} (mm^2)	d_h (mm)
PV37/PV37-2/PV37-1	139	50.4	0.37	350/250/150	400/300/200	573.1/409.4/245.6	15.4	42.0	0.550
PV65/PV65-2/PV65-1	54	50.1	0.65	350/250/150	400/300/200	385.9/275.7/165.4	17.9	42.2	0.835
PV80/PV80-2/PV80-1	32	50.2	0.80	350/250/150	400/300/200	281.5/201.1/120.6	16.1	42.2	1.032
HL31/HL31-2/HL31-1	128	50.2	0.31	350/250/150	400/300/200	436.3/311.6/187.0	9.66	42.2	0.573
HL50/HL50-2/HL50-1	85	50.5	0.50	350/250/150	400/300/200	467.3/333.8/200.3	16.7	41.9	0.681

n, number of fibres; ϕ, packing density; d_i, internal diameter of fibres; L, effective mass transfer length; L_T, total length; A_i, internal mass transfer area; A_l, A_{sh}, cross-sectional areas in the lumen side and in the shell side, respectively; d_h, equivalent hydrodynamic diameter of the shell side flow channel.

- Hausen model:

$$\mathrm{Nu_p} = \left(3.66 + \frac{0.0668\mathrm{Gz_p}}{1+0.04\mathrm{Gz_p}^{2/3}}\right) \times \left(\frac{\mu_p}{\mu_{pm}}\right)^{0.14} \quad \text{if}$$

$$\mathrm{Gz_p} = \mathrm{Re_p Pr_p}\frac{d_{hp}}{L} < 100 \qquad (14^b)$$

In both models, the subscript (p) stands for the permeate stream.

4.1. Stage 1 of model development

This stage aimed to develop a semi-empirical model, relating the hydrodynamic conditions of the system to heat and mass transfer in DCMD, in the form of Eq. (15) where constant $\bar{A}$, and the exponents α and β, were to be determined by sequentially solving heat and mass transfer balances in the DCMD process:

$$\mathrm{Nu_f} = \bar{A}\mathrm{Re_f^{\alpha}Pr_f^{\beta}}\left(\frac{\mu_f}{\mu_{fm}}\right)^{0.14} \quad \text{and} \quad \mathrm{Sh_f} = \bar{A}\mathrm{Re_f^{\alpha}Sc_f^{\beta}}\left(\frac{\mu_f}{\mu_{fm}}\right)^{0.14} \qquad (15)$$

Following was the calculation procedure:

a. All physical properties of the feed and permeate solutions were calculated based on the bulk inlet and outlet temperatures. The convective heat transfer coefficient h_p was then calculated from Eq. (14)using an iterative method with an absolute tolerance of 0.01. The surface temperatures on both sides of the membrane: T_{pm} and T_{fm} were given by Eqs. (8)–(10).
b. Similarly, the convective heat transfer coefficient, h_f, was determined from Eq. (7) and then Nusselt and Sherwood numbers were calculated. A loop started from this step with an initial value of β equal to 0.33 and was repeated until other values of β were found to well describe both heat and mass transfer:

$$h_f = \frac{Q_f}{A_o(T_f - T_{fm})}; \quad \mathrm{Nu_f} = \frac{h_f d_{hf}}{k_f}; \quad \mathrm{Sh_f} = \frac{\mathrm{Nu_f}}{(Pr_f/Sc_f)^{\beta}}$$

c. On the feed side the convective mass transfer coefficient must be calculated as well:

$$K_f = \frac{\mathrm{Sh_f} D_{G\text{-}W}}{d_{hf}}$$

where $D_{G\text{-}W}$ is the diffusivity of glucose in water at the average temperature $T = (T_f + T_{fm})/2$ in the feed thermal boundary layer.
d. Calculate the surface concentration on the feed side, based on the 'thin film theory' applied on the external surface of the fibres as given in Eq. (3).
e. Calculate the viscosity factor on the feed side $F_f = (\mu_f/\mu_{fm})^{0.14}$ once the surface quantities T_{fm} and C_{fm} are known.
f. The exponent α and the constant $\bar{A}$ in Eq. (15) were determined from a linear regression plot of $\ln(\mathrm{Re_f}) \propto \ln[\mathrm{Nu_f}/(\mathrm{Pr_f^{\beta}}F_f)]$ with the initial value $\beta = 0.33$. This value of the exponent β is the one most widely used in the heat transfer literature when undertaking purely heat transfer investigations. This step was required to establish a framework for determination of the constant $\bar{A} = \exp(\text{intercept})$ and the exponent $\alpha = (\text{slope})$ once a value of β has been accepted.
g. In order to determine the value of β that would provide the best description of both heat and mass transfer in DCMD, repeat step (f) with different value of β. For each new value of α and $\bar{A}$ found, C_{fm}, by Eq. (3), and the surface temperatures, T_{fm}, by Eq. (16), and T_{pm} by Eq. (17) were recalculated. This was done by using the heat and mass transfer coefficients estimated by the newly obtained model and the experimentally measured data. These equations were derived by equating the heat and mass transfer balances described by Eqs. (7)–(10):

$$T_{fm} = T_f - \frac{(T_f - T_p)h_m + J\,\Delta H_v}{h_m + h_{f''}(1 + (h_m/h_p))} \qquad (16)$$

$$T_{pm} = T_p - \frac{(T_f - T_p)h_m + J\,\Delta H_v}{h_m + h_p\left(1 + \frac{h_m}{h_{f''}}\right)}; \quad \text{where} \quad h_{f''} = h_f\frac{r_o}{r_i} \qquad (17)$$

Referring to Eq. (1), coefficient K_m, the membrane water vapour permeability, could be varied slightly due to its dependence on the temperature of the membrane wall. Two linear regression curves describing heat and mass transferred were plotted, with R^2_{mass} and R^2_{heat}, coefficients of determination for mass and heat transfer, respectively:

- $J \propto \Omega\,\Delta P_m = \Omega(P_{fm} - P_{pm})$; with R^2_{mass}.
- $Q_{cond} = (Q_m - A_i J\,\Delta H_v) \propto \Delta T_m = T_{fm} - T_{pm}$; with R^2_{heat}.

The slopes of the regression curves respectively represented the membrane structural parameter K_M, as defined in Eq. (2), and the products of $(A_i h_m)$. The best value of β would maximise the sum $(R^2_{mass} + R^2_{heat})$, which could simultaneously describe heat and mass transfer in the DCMD process. An example of these linear regression plots will be presented in Fig. 5 of the result and discussion section.

4.2. Stage 2 of model development

This stage aimed to include the effect of the module's length on heat and mass transfer. In each type of the hollow fibre module investigated in this work, length was the only structural parameter being varied. Consequently, it could be assumed that the effects of the hydrodynamic conditions (indicated by α) and the ratio of momentum diffusivity over heat and mass diffusivity (indicated by β) on DCMD heat and mass transfer were the same regardless of the module length within the range from 150 to 350 mm. Therefore, a new model represented by Eq. (18), having the same α and β as in Eq. (15), was developed to include a new term (d_{hf}/L) which could describe the effect of the length of the module:

$$\mathrm{Nu_f} = \bar{B}\mathrm{Re_f^{\alpha}Pr_f^{\beta}}\left(\frac{d_{hf}}{L}\right)^{\varphi}\left(\frac{\mu_f}{\mu_{fm}}\right)^{0.14} \text{and } \mathrm{Sh_f} = \bar{B}\mathrm{Re_f^{\alpha}Sc_f^{\beta}}\left(\frac{d_{hf}}{L}\right)^{\varphi}\left(\frac{\mu_f}{\mu_{fm}}\right)^{0.14} \qquad (18)$$

Experiments in the second stage working with the short module groups of all types of hollow fibre were modified to work at two ini-

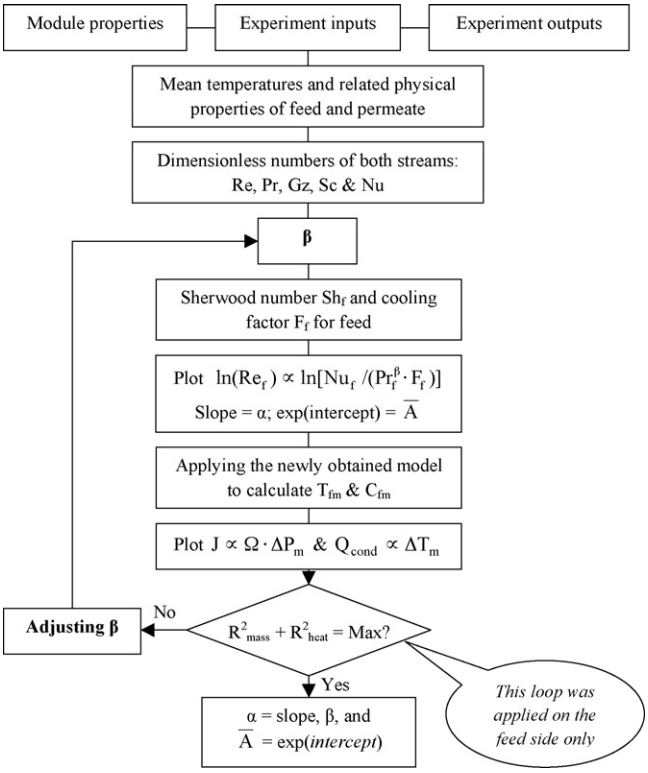

Fig. 4. Construction of the spreadsheet for model development in stage 1.

tial feed concentrations, C_f = 30 and 35% (w/w), two feed velocities, ω_f = 0.4 and 0.8 m s^{-1}, and one feed inlet temperatures, T_{fi} = 35 °C. The designed experiments would yield enough data points to investigate the effect of module length on heat and mass transfer. Steps a–e of stage 1 were repeated with known α and β. Finally, a linear regression plot of $\ln[Nu_f/(Re_f^{\alpha}Pr_f^{\beta}F_f)] \propto \ln(d_{hf}/L)$ was created, to obtain φ = slope and $\bar{B}$ = exp(intercept) of the regression curves.

5. Results and discussion

Microsoft-Excel spreadsheets were constructed to process the calculations in stage 1, as scheduled in Fig. 4. The best value of β, $\bar{A}$ and α in the heat and mass transfer models for the feed side, as shown in Eq. (15) were found. The procedure was applied for the feed side only. For each value of β, the plots $J \propto \Omega\,\Delta P_m$ and $Q_{cond} \propto \Delta T_m$ were observed, and coefficients of determination R^2_{mass}, R^2_{heat} and their sum were recorded.

It was found that increasing β from 0.30 to 1.00 improved the linearity of the plot $\ln(Re_f) \propto \ln[Nu_f/(Pr_f^{\beta}F_f)]$, but rapidly worsened the linearity of the plots $J \propto \Omega\,\Delta P_m$ and $Q_{cond} \propto \Delta T_m$ when β became greater than 0.60. Two examples of the mentioned plots due to different values of the exponent β are shown in Figs. 5 and 6. It could be concluded that good linearity of the plot $\ln(Re_f) \propto \ln[Nu_f/(Pr_f^{\beta}F_f)]$ does not necessarily mean that the model derived from that plot could adequately describe the simultaneous heat and mass transfer in DCMD.

The effect of β on the sum of $(R^2_{mass} + R^2_{heat})$ is illustrated in Fig. 7, and the best β was picked at its peak. At these values of β, details of the models developed are listed in Table 3. The obtained values of β showed that 0.33 was no longer the most suitable exponent for the Prandtl and Schmidt numbers in DCMD, due to the simultaneous occurrences of heat and mass transfer. It appeared that the best β was influenced by not only the mass flux, but also the type of hollow fibres. One possible explanation is that higher mass flux

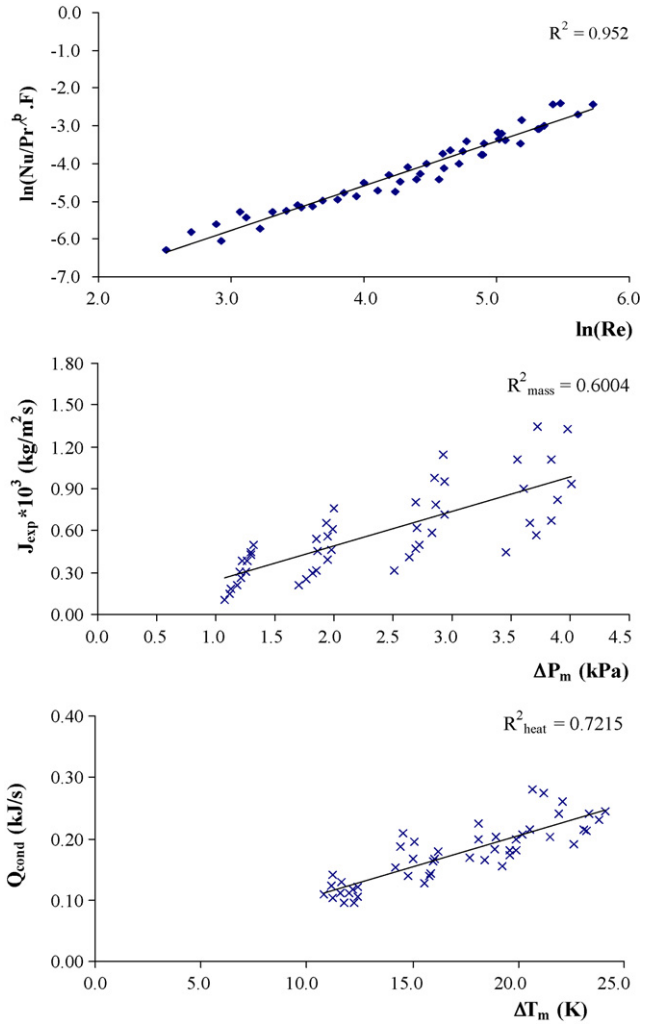

Fig. 5. Plots $\ln(Re_f) \propto \ln[Nu_f/(Pr_f^{\beta}F_f)]$, $J \propto \Omega\,\Delta P_m$, and $Q_{cond} \propto \Delta T_m$ at β = 1.00 for module HL50.

leads to a thicker concentration boundary layer on the feed side. This also affects the thermal boundary layer, due to the heat transport associated with mass transfer. Thus, the role of the Schmidt and Prandtl numbers in the model was influenced by mass transfer in DCMD, and eventually meant adopting new values for β other than 0.33, depending on the mass transfer rates achieved by each type of hollow fibre.

The geometry parameter $\bar{A}$ in the models varied considerably amongst the modules. This was probably due to the differences of the fibre sizes, their physical properties, and their distribution within the shell. The obtained exponents α, ranging from 0.63 to 1.06, indicated that the flow through the shell side was in the transitional to turbulent regime, even though the highest Reynolds number was only 470. This phenomenon was due to tortuosity of the hollow fibres in the bundle. More tortuous fibres had a higher

Table 3
The semi-empirical models as in Eq. (15) developed in stage 1.

Module	$10^3*\bar{A}$	α	β	R^2
PV80	25.91	0.63	0.38	0.9327
PV65	8.56	0.75	0.39	0.9478
PV37	2.27	1.06	0.55	0.9580
HL50	7.68	0.64	0.45	0.8874
HL31	7.50	0.68	0.42	0.8594

R^2, coefficient of determination of $\ln(Re_f) \propto \ln[Nu_f/(Pr_f^{\beta}F_f)]$ plot.

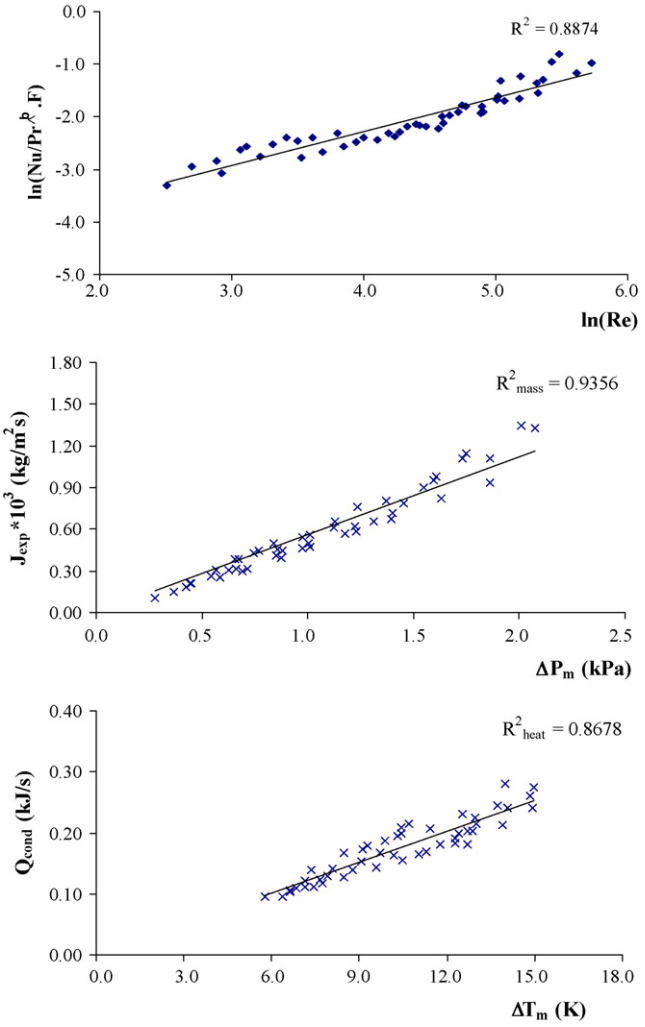

Fig. 6. Plots $\ln(Re_f) \propto \ln[Nu_f/(Pr_f^{\beta}F_f)]$, $J \propto \Omega\,\Delta P_m$, and $Q_{cond} \propto \Delta T_m$ at $\beta = 0.45$ for module HL50.

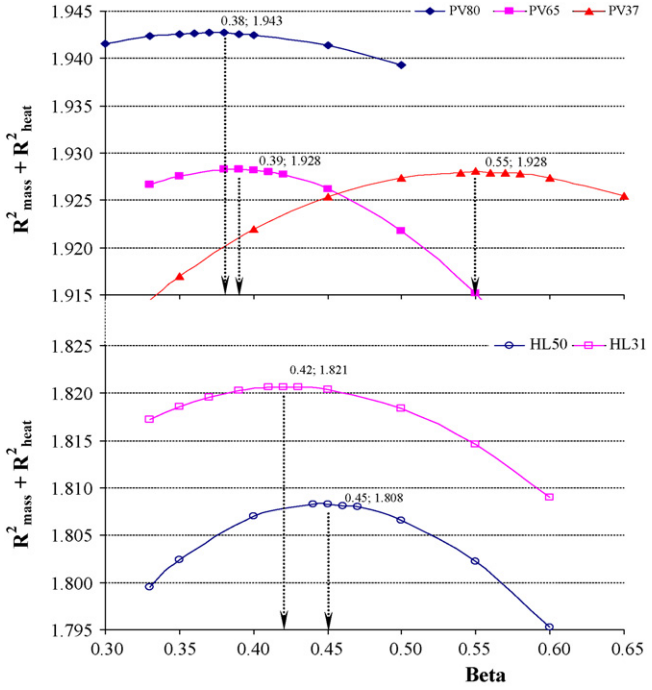

Fig. 7. Effect of exponent β on the overall description of heat and mass transfer by the semi-empirical models developed in stage 1.

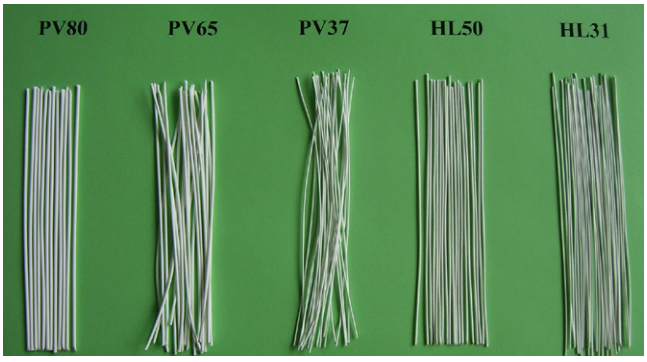

Fig. 8. Image of randomly taken bundles of the studied hollow fibres.

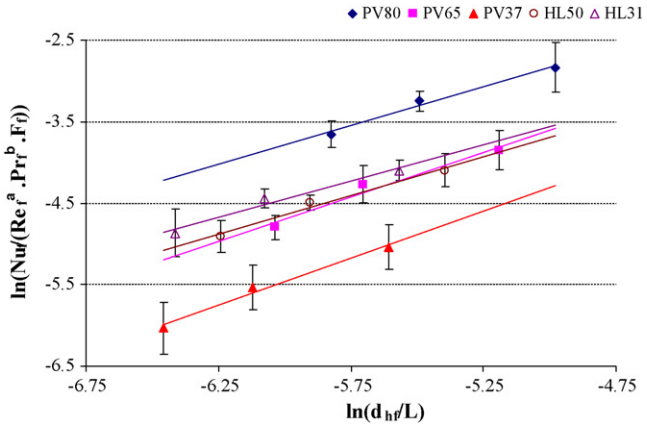

Fig. 9. Effect of length on heat and mass transfer in HFMs (error bars are standard deviations of the data).

likelihood of causing turbulence than the others, hence produced a higher value of α. As shown in Fig. 8, fibres PV37 and PV65 were much more tortuous than the others, and consequently, much higher values of α were obtained for them. Fibres PV80, HL50 and HL31 were of similar straightness, hence their exponents α were almost the same.

Calculations for stage 2 were carried out in similar ways, which included all the data on modules of all lengths. Then, the plot of $\ln[Nu_f/(Re_f^{\alpha}Pr_f^{\beta}F_f)] \propto \ln(d_{hf}/L)$ was created, with Nu_f being the experimental Nusselt number of the feed flow, and α and β being the newly obtained exponents in stage 1. This plot is shown in Fig. 9. The slopes and intercepts of the lines were then taken to estimate the exponent φ and the constants $\bar{B}$ in model Eq. (18) accordingly. The graph showed that under similar operating conditions, heat and mass transfer were more intensive in shorter modules. This phenomenon was expected, since shorter modules meant a shorter contact time of the fluids with the membrane surface, resulting in a smaller drop in the fluids' temperatures while flowing through the membrane module. As a result, the transmembrane temperature difference was higher in short modules than in the long ones when the same operating conditions were applied, thus more intensive heat and mass transfer occurred.

Details of the final models are listed in Table 4. It can be seen that the exponent φ for all the modules were relatively comparable to each other, and varied around unity.

Table 4
The semi-empirical models as in Eq. (18) for heat and mass transfer in DCMD.

Module	$\bar{B}$	α	β	φ	R^2
PV80	7.03	0.63	0.38	0.96	0.9867
PV65	6.42	0.75	0.39	1.09	0.9647
PV37	4.39	1.06	0.55	1.16	0.9857
HL50	2.83	0.64	0.45	0.95	0.9786
HL31	2.41	0.68	0.42	0.89	0.9671

R^2, coefficient of determination of the lines in Fig. 9.

The outcome of exponent φ being higher than α in all cases indicated that length had a greater effect on heat and mass transfer in DCMD than the Reynolds number. In other words, reducing the length, L (or increasing d_{hf}/L), was more effective than increasing the feed velocity at improving the rate of heat and mass transfer. Moreover, the ratio (φ/α) appeared to be proportional to the straightness of the fibres and the equivalent diameter, d_{hf}, of the feed flow channel, highlighting the more important role of length in, for example, module PV80 than in PV37. Reducing the module's length may not be an economical or practical solution in the DCMD concentration operation, but increasing the diameter of the feed flow channel could be considered to improve the heat and mass transfer.

The validity of the newly developed models was assessed by the linearity of the plots between the heat and mass fluxes versus their corresponding transmembrane driving forces as shown in Fig. 10. For comparison purpose, this assessment was also carried out for the heat transfer model proposed by Kreith and Bohn [30] since it had been used by Khayet et al. [21] for analysing DCMD heat and mass transfer in the shell side of a hollow fibre module. The plots in Fig. 10 clearly showed that the newly developed models could better describe both heat and mass transfer in DCMD than the one proposed by Kreith and Bohn. This is an indication that the new modelling method offered in this study is more advantageous than using non-linear regression softwares since it correlates two sets of data for heat and mass transfer simultaneously, while not violating the theory of their analogy.

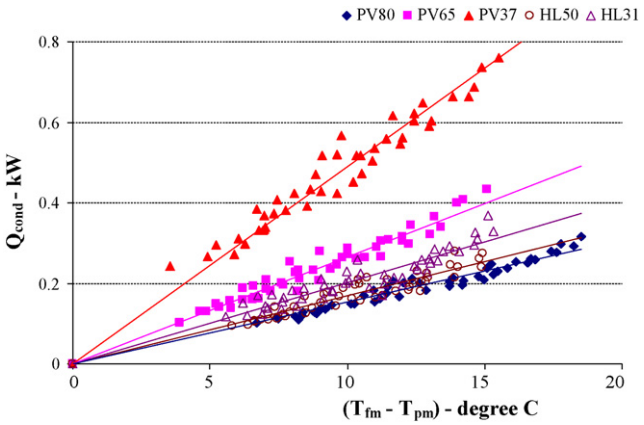

Fig. 11. Linearity between conductive heat flux and transmembrane temperature difference.

Applying the newly developed models Eq. (18) resulted in a relatively good linearity for the plots $Q_{cond} \propto \Delta T_m$ and $J \propto \Omega\, \Delta P_m$. These graphs are shown in Figs. 11 and 12, with the slopes respectively indicating the products of the membrane area and its thermal conductivity ($A_i h_m$), and the structural parameter, K_M, of the corresponding fibres. It is desirable that the DCMD process be operated at minimum heat loss with maximum mass flux across the membrane from the feed to permeate. In other words, a membrane considered suitable for DCMD, must possess the combined properties of high heat resistance and high vapour permeability. Clearly, hollow fibre PV80 appeared to be the least vapour-permeable membrane, and is therefore not suited in DCMD application, when mass flux is the main concern. Hollow fibre PV37 was highly thermally conductive and possessed the second least vapour-permeable property, and is therefore also not suitable for DCMD application. Halar fibres HL50 and HL31, with their heat resistance close to that of PV80, the highest amongst the five types of fibres tested, yet far better

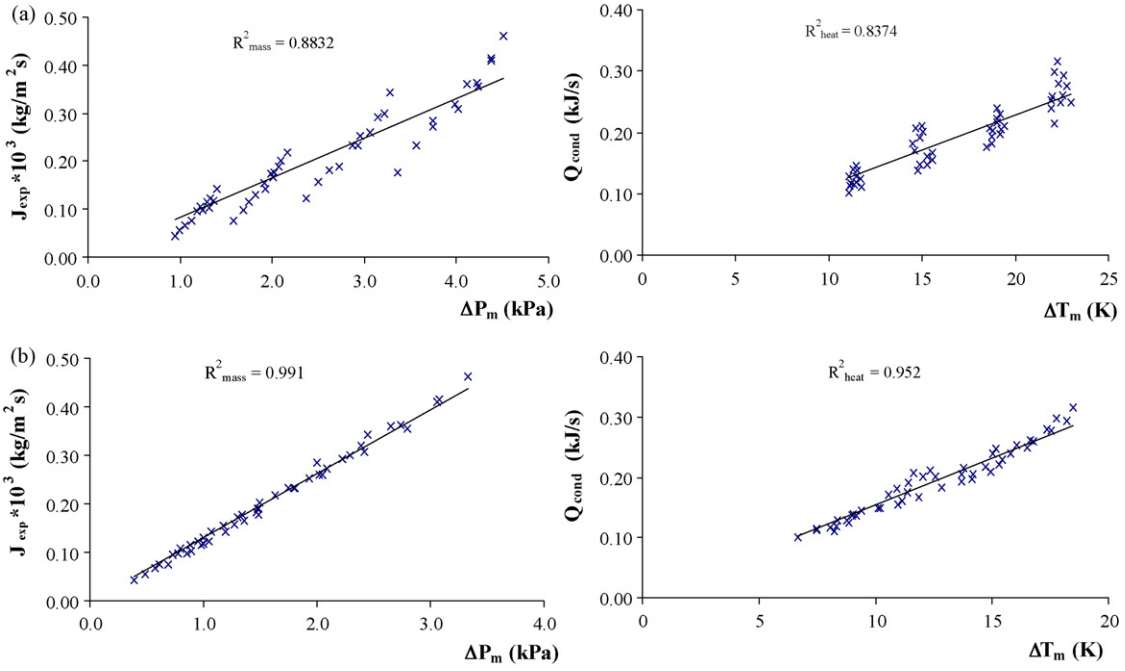

Fig. 10. Linear relationship between mass and heat fluxes versus their corresponding transmembrane driving forces by the models for module PV80. (a) By model proposed by Kreith and Bohn [30] and (b) by model developed in this study.

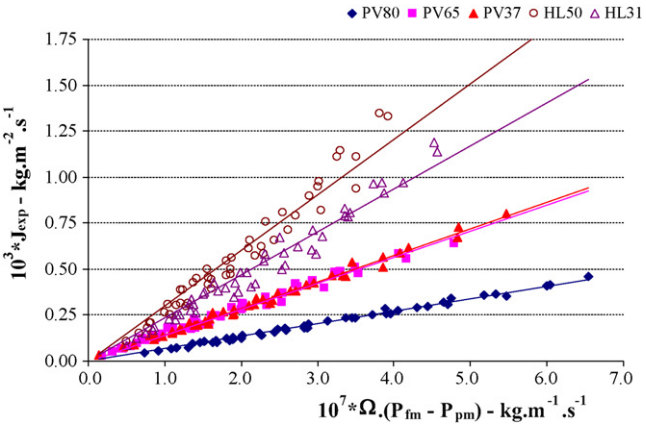

Fig. 12. Linearity between mass flux and transmembrane water vapour pressure difference.

vapour permeability, seemed to be the most desirable membranes amongst the studied hollow fibres for DCMD.

6. Conclusions

A procedure for modelling transport processes in DCMD within a hollow fibre module was developed, by adopting the analogy between heat and mass transfer in a dimensional analysis framework. Models in the form of $Nu = \bar{B}Re^{\alpha}Pr^{\beta}(d_h/L)^{\varphi}(\mu_b/\mu_m)^{0.14}$ and $Sh = \bar{B}Re^{\alpha}Sc^{\beta}(d_h/L)^{\varphi}(\mu_b/\mu_m)^{0.14}$ were developed in this study, to describe the simultaneous heat and mass transfer in DCMD. The exponent, α in the models, indicating the hydrodynamic conditions, were found to be indirectly proportional to the tortuosity of fibres in the bundle. The results showed that $\beta = 0.33$ was no longer the most suitable exponent for the Prandtl number in a semi-empirical model for heat transfer in DCMD. Indeed, β, indicating the ratio of momentum diffusivity over heat and mass diffusivity, may vary due to the specific conditions of the system, especially the mass transfer rate. At high mass transfer rate, the values of β were higher than 0.33 and could be up to 0.55 as found in our experiments. The models developed in this work successfully described heat and mass transfer in DCMD and showed linear relationships between heat and mass transfer rates and their respective driving forces. They also showed that the effect of fibre length could, under some circumstances, be greater than that of velocity on heat and mass transfer.

Heat and mass transfer analysis by the newly developed models showed that amongst the studied membranes, Halar fibres possessed the combinational qualities that were desirable for an efficient DCMD operation. These qualities included the co-occurring low thermal conductivity (heat resistant) and high vapour permeability (mass conductive). In contrast, PVDF fibres were found to be either heat resistant but mass resistant (PV80) or mass conductive but heat conductive (PV37), or in-between the two extremes (PV65) and therefore not desirable in DCMD.

Acknowledgements

The authors would like to thank University of Western Sydney for the International Postgraduate Research Scholarship for Viet Bui, Siemens Water Technology, Australia for supporting the project with hollow fibres, Dr. J. Muller for technical advice and Dr. J. Hourigan for editorial advice.

Appendix A. Nomenclatures

Capital letters

A_i, A_o	internal, external surface area of hollow fibres (m^2)
C	concentration of a solution (%, w/w)
C_{px}	specific heat capacity of material in the (x) domain ($J\,kg^{-1}\,K^{-1}$)
$D_{G\text{-}W}$	diffusivity of glucose in water ($m^2\,s^{-1}$)
$D_{w\text{-}air}$	diffusivity of water vapour through stagnant air ($m^2\,s^{-1}$)
F_f	viscosity factor on the feed side
J	mass flux ($kg\,m^{-2}\,s^{-1}$)
K_f	convective mass transfer coefficient on the feed side ($m\,s^{-1}$)
K_1	membrane quality parameter, $K_1 = \varepsilon/\tau$
K_M	membrane structural parameter
K_m	membrane's vapour permeability ($kg\,m^{-2}\,s^{-1}\,Pa^{-1}$)
M	water molecular weight ($kg\,kmol^{-1}$)
P	water vapour pressure (Pa)
Q^x	heat flux gained or lost by the (x) stream (x = F for feed or x = P for permeate) (W)
Q_x	heat flux across the (x) domain (W)
Q_{diff}	heat flux due to mass diffusion (W)
Q_{cond}	heat flux due to conduction (W)
Q_T	total heat flux (W)
R	universal gas constant ($m^3\,Pa\,kg\,mol^{-1}\,K$)
T	temperature (°C or K)
U	overall heat transfer coefficient ($W\,m^{-2}\,k^{-1}$)
Y_{lm}	log-mean molar fraction of air in membrane pores

Lower case letters

a_w	water activity of a solution
h	heat transfer coefficient ($W\,m^{-2}\,K^{-1}$)
k	thermal conductivity ($W\,m^{-1}\,K^{-1}$)
$\dot{m}$	mass flow rate of a stream ($kg\,s^{-1}$)
r_i/r_o	internal/external radius of hollow fibres (m)

Greek letters

ΔH_v	latent heat of vapourisation of water ($J\,kg^{-1}$)
ΔP_x	vapour pressure difference across x-domain
α, β, φ	exponents in semi-empirical models
ε	membrane porosity
μ	viscosity (Pa s)
ρ	density ($kg\,m^{-3}$)
τ	membrane pore tortuosity
ω	fluid velocity ($m\,s^{-1}$)

Subscripts

air	air
b	in the bulk
f	feed or feed domain
fm	at feed membrane surface
fi, fo	feed inlet, outlet
m	membrane, or membrane surface
p	permeate or permeate domain
pl	membrane polymer
pm	at permeate membrane surface
pi, po	permeate inlet, outlet

Dimensionless numbers used in semi-empirical equations

Nu	Nusselt number
Gz	Graetz number
Pr	Prandtl number
Re	Reynolds number
Sh	Sherwood number
Sc	Schmidt number

References

[1] R.W. Schofield, A.G. Fane, C.J.D. Fell, Heat and mass transfer in membrane distillation, J. Membr. Sci. 33 (3) (1987) 299–313.
[2] M.S. El-Bourawi, Z. Ding, R. Ma, M. Khayet, A framework for better understanding membrane distillation separation process, J. Membr. Sci. 285 (1–2) (2006) 4–29.
[3] A.M. Alklaibi, N. Lior, Membrane-distillation desalination: status and potential, Desalination 171 (2) (2004) 111–131.
[4] F. Lagana, G. Barbieri, E. Drioli, Direct contact membrane distillation: modelling and concentration experiments, J. Membr. Sci. 166 (1) (2000) 1–11.
[5] V.A. Bui, M.H. Nguyen, J. Muller, Challenge and opportunity of direct contact membrane distillation in liquid food concentration, in: B.R. Young, D.A. Patterson, X.D. Chen (Eds.), Chemeca 2006, Engineers Australia, Auckland, New Zealand, 17–21st September, 2006 (Article 137).
[6] E. Curcio, G. Barbieri, E. Drioli, Operazioni di distillazione a membrana nella concentrazione dei succhi di fruitta, Industrie delle Bevande 29 (April) (2000) 113–120.
[7] V.D. Alves, I.M. Coelhoso, Orange juice concentration by osmotic evaporation and membrane distillation: a comparative study, J. Food Eng. 74 (1) (2006) 125–133.
[8] L. Martinez-Diez, F.J. Florido-Diaz, M.I. Vazquez-Gonzalez, Study of evaporation efficiency in membrane distillation, Desalination 126 (1–3) (1999) 193–198.
[9] V.A. Bui, M.H. Nguyen, J. Muller, The energy challenge of direct contact membrane distillation in low temperature concentration, Asia-Pacific J. Chem. Eng. 2 (5) (2007) 400–406.
[10] M. Khayet, M.P. Godino, J.I. Mengual, Possibility of nuclear desalination through various membrane distillation configurations: a comparative study, Int. J. Nucl. Desalination 1 (1) (2003) 30–46.
[11] M.A. Izquierdo-Gil, C. Fernandez-Pineda, M.G. Lorenz, Flow rate influence on direct contact membrane distillation experiments: different empirical correlations for Nusselt number, J. Membr. Sci. 321 (2008) 356–363.
[12] L. Martinez, J.M. Rodriguez-Maroto, Characterization of membrane distillation modules and analysis of mass flux enhancement by channel spacers, J. Membr. Sci. 274 (1–2) (2006) 123–137.
[13] C. Fernandez-Pineda, M.A. Izquierdo-Gil, M.C. Garcia-Payo, Gas permeation and direct contact membrane distillation experiments and their analysis using different models, J. Membr. Sci. 198 (1) (2002) 33–49.
[14] V.A. Bui, M.H. Nguyen, J. Muller, Prediction of water activity of glucose and calcium chloride solutions, J. Food Eng. 57 (3) (2003) 243–248.
[15] L.N. Bell, T.P. Labuza, Moisture Sorption––Practical Aspects of Isotherm Measurement and Use, 2nd ed., American Association of Cereal Chemists Inc., 2000.
[16] R.W. Schofield, A.G. Fane, C.J.D. Fell, Gas and vapour transport through microporous membranes. I. Knudsen–Poiseuille transition, J. Membr. Sci. 53 (1–2) (1990) 159–171.
[17] C.M. Guijt, G.W. Meindersma, T. Reith, A.B. de Haan, Method for experimental determination of the gas transport properties of highly porous fibre membranes: a first step before predictive modelling of a membrane distillation process, Desalination 147 (1–3) (2002) 127–132.
[18] S. Ma, L. Song, S.L. Ong, W.J. Ng, A 2-D streamline upwind Petrov/Galerkin finite element model for concentration polarization in spiral wound reverse osmosis modules, J. Membr. Sci. 244 (1–2) (2004) 129–139.
[19] A. Subramani, S. Kim, E.M.V. Hoek, Pressure, flow, and concentration profiles in open and spacer-filled membrane channels, J. Membr. Sci. 277 (1–2) (2006) 7–17.
[20] A.M. Alklaibi, N. Lior, Comparative study of direct-contact and air-gap membrane distillation processes, Ind. Eng. Chem. Res. 46 (2) (2007) 584–590.
[21] M. Khayet, M. Godino, J. Mengual, Study of asymmetric polarization in direct contact membrane distillation, Sep. Sci. Technol. 39 (1) (2004) 125–147.
[22] L. Martínez-Díez, F.J. Florido-Díaz, M.I. Vázquez-González, Study of polarisation phenomena in membrane distillation of aqueous salt solutions, Sep. Sci. Technol. 35 (10) (2000) 1485–1501.
[23] V.A. Bui, M.H. Nguyen, J. Muller, Characterisation of the polarisations in osmotic distillation of glucose solutions in hollow fibre module, J. Food Eng. 68 (3) (2005) 391–402.
[24] J.I. Mengual, J.M. Ortiz de Zarate, L. Pena, A. Velazquez, Osmotic distillation through porous hydrophobic membranes, J. Membr. Sci. 82 (1–2) (1993) 129–140.
[25] R.B. Bird, W.E. Stewart, E.N. Lightfoot, Transport Phenomena, 2nd ed., John Wiley & Sons Inc., USA, 2002.
[26] C.J. Geankoplis, Transport Processes and Separation Process Principles (Includes Unit Operations), 4th ed., Prentice Hall Inc., Upper Saddle River, New Jersey, USA, 2003.
[27] M.N. Ozisik, Heat Transfer—A Basic Approach. Mech. Eng. Series, McGraw-Hill International Editions, Singapore, 1985.
[28] F.M. White, Heat and Mass Transfer, Addison-Wesley Publishing Company, Inc, USA, 1991.
[29] W.L. McCabe, J.C. Smith, P. Harriott, Unit Operations of Chemical Engineering. Chem. Eng. Series, 4th ed., McGraw-Hill International Editions, 1985.
[30] F. Kreith, M.S. Bohn, Principles of Heat Transfer, 5th ed., PWS Publishing Company, ITP Inc., Boston, 1997.